Functional Materials Letters
Vol. 10, No. 3 (2017) 1750012 (5 pages)

DOI: 10.1142/S1793604717500126

Transmission electron microscopy characterization of protective $La_{0.7}Sr_{0.3}MnO_{3-\delta}$ coatings prepared by electrostatic spray deposition on ferritic alloy

Leandro da Conceição*,†,§, Sabine Lay‡, Florence Robaut‡, Gilles Renou‡, E. N. S. Muccillo† and Elisabeth Djurado*

*Universite Grenoble Alpes, CNRS
LEPMI, F-38000 Grenoble, France

†Energy and Nuclear Research Institute-IPEN
P. O. Box 11049, S. Paulo, 05422-970, SP, Brazil

‡Universite Grenoble Alpes, CNRS, SIMAP
F-38000 Grenoble, France
§landoufrj@gmail.com

Received 5 July 2016; Accepted 23 November 2016; Published 30 December 2016

The effect of $La_{0.7}Sr_{0.3}MnO_{3-\delta}$ (LSM) coating on SS446 steel on air oxidation at 800°C was investigated by transmission electron microscopy. Dense and crack free thin LSM films were prepared by electrostatic spray deposition. The microstructural characterization was carried out on coated and uncoated interconnectors. A thin chromia scale at the alloy interface along with two spinel phases were observed after long term oxidation in both cases. Specimens exhibit, in addition, an SiO_2 layer at the interface with steel due to the high content of Si in the steel. Significant changes in the thickness, morphology and composition occurred in the reaction layer for the LSM coated steel. These effects are explained on the basis of changes in the diffusive fluxes during exposure to the oxidation treatment. The implications of these effects for the degradation mechanism of LSM-based interconnects are discussed.

Keywords: Lanthanum manganite; transmission electron microscopy; electrostatic spray deposition; interconnects; solid oxide fuel cell.

Recent progress in the manufacturing of thin layers of ceramic electrolytes has enabled reduction of the operating temperature of solid oxide fuel cells (SOFCs) to 600–800°C, allowing the use of metallic interconnects with consequent reduction in the production cost.[1]

The highly alloyed steels for this application are known to develop a slow growing chromia-rich scale that inhibits fast corrosion of the metal at high temperatures. Nevertheless, the gradual increase of the electrical resistance with time and the evaporation of volatile chromium species lead to degradation of the stack performance, limiting its lifetime.[2] The evaporation of chromium species is known to be responsible for the contamination of the interface between the cathode and the electrolyte by blocking the catalytic reactive sites.[2] To overcome these deleterious effects, alloyed steels, which are able to develop a $(Cr,Mn)_3O_4$ spinel phase on the chromia layer have been investigated. It has been already shown that this spinel layer is able to reduce the Cr volatilization by approximately 50%.[3,4] Further reduction of Cr volatilization would be attractive to minimize its reaction with the adjacent cathode, avoiding the consequent decrease of power density.[5]

Deposition of thin protective coatings on alloy interconnects is recognized to improve the suitability of chromia forming alloys.[3,4,6–8] Protective coatings on ferritic steels are known to decrease both the oxidation rate of the chromia forming alloys and the electrical resistance of the produced oxides. Moreover, the protective coatings have been shown to reduce the chromium evaporation and diffusion from the oxide surface during long-term device operation.[1,5–8] An important concern is the growth of an interfacial reaction layer, which may occur during high temperature fabrication of coatings, and is usually found between the coating and the alloy or the chromia oxide scale. The composition of the interfacial layer depends on the coating itself. For example, when the coating was $(Mn,Co)_3O_4$, the interfacial layer consisted of $(Mn,Co,Cr)_3O_4$.[6]

§Corresponding author.

The perovskite mixed oxides based on strontium-doped lanthanum manganite ($La_{0.7}Sr_{0.3}MnO_{3-\delta}$ (LSM)), cobaltite or chromite, which are chemically and thermally compatible with other components in SOFC devices, are candidates for deposition as coatings on alloy-based interconnects. To date, few microstructure reports are available on the chromium retention by protective perovskite coatings. Spinel containing manganese interfacial layers are likely to be promising as protective coating on ferritic steels,[1,2,6–8] and a comprehensive characterization of the microstructure of these coated steels is required for designing optimized metallic interconnectors.

In this work, the results of a microstructural study on LSM-coated SS446 steel are reported. For comparison purposes, the uncoated steel was investigated as well. Several crystalline phases in these samples were characterized by electron diffraction and X-ray energy dispersive spectroscopy (EDS) coupled to a transmission electron microscopy (TEM). Based on the obtained results, the mechanisms responsible for the formation of the reaction layers are discussed in addition to their influences on the overall lifetime and performance of SOFCs.

Experimental Details: Coating Preparation. LSM thin films were deposited by electrostatic spray deposition (ESD) on polished SS446 stainless steel (Ugitech, France) with dimensions of $\phi 20\,\text{mm} \times 1\,\text{mm}$ thickness. The chemical composition of SS446 steel is shown in Table 1. The surface of substrates was suitably treated before deposition as described elsewhere.[8]

The coating films were deposited in a vertical ESD setup,[8,9] starting from $La(NO_3) \cdot 6H_2O$, $SrCl_2 \cdot 6H_2O$, and $Mn(NO_3)_3 \cdot 6H_2O$ and a mixture of 67:33 vol.% ratio of ethanol (C_2H_5OH, 99.9%) and butyl carbitol ($CH_3(CH_2)_3OCH_2CH_2OCH_2CH_2OH$, 99%) named EtOH and BC, respectively, with concentration of $0.02\,\text{mol} \cdot \text{L}^{-1}$. Details of coatings fabrication by ESD have been reported elsewhere.[8] The coated steel was found amorphous by X-ray diffraction and a subsequent annealing at 800°C for 2 h in air was performed for film crystallization. Dense films, free of cracks, and as thin as 450 nm have been successfully deposited by ESD on SS446. The oxidation experiments were carried out at 800°C in air for 200 or 480 h. The required long oxidation times, even though arbitrarily chosen, yielded consistent interpretation of the experimental data.

Table 1. Chemical composition (wt.%) of ferritic SS446 stainless steel used as a substrate.

Sample	Fe	Cr	Mn	Si	Mo	V	W	Ni	Cu
SS446	Bal.	23.15	0.53	0.36	0.07	0.11	0.02	0.20	0.15

Coating Characterization. The microstructure of the films developed on the SS446 stainless steel surface after corrosion experiments was investigated by TEM using a 2100F Jeol microscope equipped with an energy dispersive X-ray (EDX) system.

Cross-sectional thin foils were prepared by focused ion beam (FIB) using a Zeiss NVision 40 instrument equipped with a gallium ion source operating in the accelerating voltage range 1–30 kV. *In situ* carbon and tungsten depositions were carried out to protect the surface of the TEM specimen during FIB preparation. Final thinning was conducted with a low voltage of 3 keV and a Ga^+ beam current of a few tens of pA to reduce beam damage of the material.

The oxide scale composition was determined by EDX mapping using a beam size of 1 nm and a step size of 4 or 8 nm. In addition, the automated crystal orientation and phase mapping (ACOM) technique usually referred as ASTAR™ technique was used to determine the distribution of the phases in the oxide scales.[10] This method is based on the acquisition of diffraction patterns by scanning the TEM samples with a nano-beam and on the recognition of the diffraction patterns using a template matching procedure. In this study, diffraction pattern quality was enhanced using beam precession with an angle of 1.2° and scanning was performed with a 3 nm step size. The experimental data were interpreted using the ICDD files 04-008-6181 (Cr_2O_3), 04-002-3807 ($(Cr,Mn)_3O_4$ and 04-015-2353 (LSM). Chromia presents a rhombohedral unit cell with $a = 0.496\,\text{nm}$ and $c = 1.3598\,\text{nm}$. The spinel phase is cubic with lattice parameter $a = 0.8460\,\text{nm}$, and the unit cell of LSM is characterized by a rhombohedral structure with $a = 0.5505\,\text{nm}$ and $c = 1.3355\,\text{nm}$.

Microstructural analysis was carried out on two cross-sections: the uncoated alloy after oxidation at 800°C for 200 h in air, and the LSM-coated alloy after oxidation at 800°C for 480 h in air.

Results and discussion. Figure 1 shows for comparison a TEM bright field image of the studied samples. An oxide scale is observed on the surface of the uncoated steel after oxidation at 800°C for 200 h. Its thickness is slightly thinner than the layer found at the surface of the LSM coated steel oxidized at 800°C for 480 h. The microstructure of the scales in both samples is detailed in the following.

Uncoated SS446 steel after oxidation for 200 h. Figure 2 shows the uncoated SS446 steel after oxidation at 800°C in air for 200 h. A thin and continuous film with white contrast may be observed at the interface with the steel and could be assigned to SiO_2. Under this film, the presence of Cr_2O_3 layer about 300 nm in thickness with fine grain size is detected. Below, $(Cr,Mn)_3O_4$ spinel appears with larger grain size

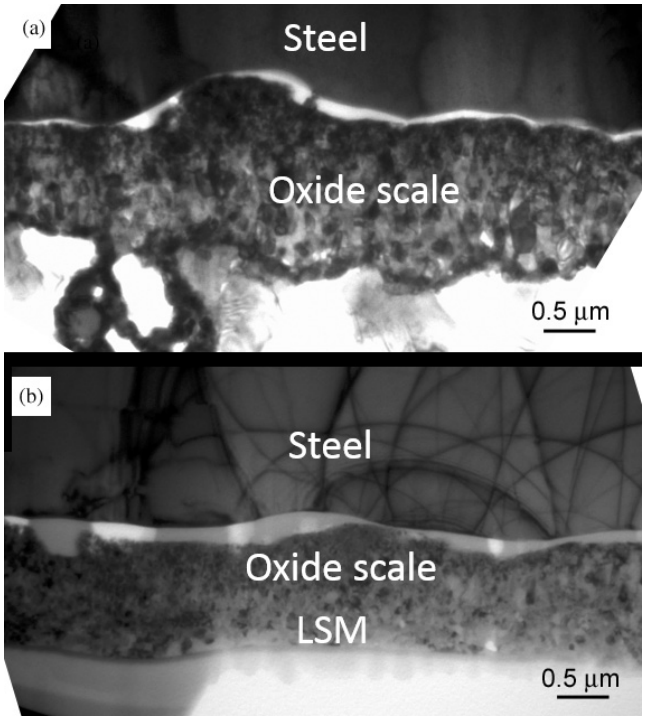

Fig. 1. TEM bright field images of a cross-section of the oxide scale formed at 800°C in air (a) on the uncoated sample after 200 h and (b) on the LSM coated sample after 480 h.

(Table 2). A careful inspection of the EDX profile shows that the oxide scale close to the surface is characterized by Mn-rich $(Cr,Mn)_3O_4$ spinel grains.

The transition from steel to oxide scale is depicted in Fig. 3 where EDX mapping of elements and phases are shown for the same area. Both chemical and crystallographic data are combined to fully characterize the sequence of layers. Electron diffraction patterns arising from SiO_2 film denote an amorphous phase (Fig. 3(g)). Just below, the Cr_2O_3 phase is identified in brown. The chemical profile of the Cr_2O_3 layer shows the presence of a rather constant amount of Mn (Fig. 2(b)). It agrees with a small solubility of Mn in chromia.[11] One can notice the presence of some spinel grains in green in the Cr_2O_3 layer. However, the phase reliability value associated with these small grains is often low (Fig. 3(h)) and no Cr and Mn variations are seen in the respective Cr and Mn maps at the interior of Cr_2O_3 layer (Figs. 3(e) and 3(f)). The TEM thin foil is rather thick, probably containing several Cr_2O_3 grains in depth and consequently leads to a low reliability of the ACOM method.[11] It is therefore very likely that no spinel grains are present in the Cr_2O_3 layer. Then, the $(Cr,Mn)_3O_4$ spinel phase is detected from electron diffraction in agreement with chemical analyses. This layer contains a small amount of Cr_2O_3 grains which are also observed on the EDX maps. Moreover, the grain size in the spinel layer is much larger than in the Cr_2O_3 layer (Fig. 3(i), Table 2).

The amorphous silica layer is due to the relatively high Si content of the commercial SS446 steel (Si-0.36%). The interfacial oxide phases found in this work for uncoated steel were also identified by corrosion studies,[1] showing that the oxide scale consists essentially of Cr_2O_3 and $(Cr,Mn)_3O_4$ layers. The amount of this spinel phase is largely determined by the available Mn content in the system.[1]

According to the phase diagram of Cr–Mn–O,[11] the composition of the cubic spinel in equilibrium with Cr_2O_3 is close to that of Cr_2MnO_4. This is in general agreement with the observation of stoichiometric Cr_2MnO_4 on the Cr_2O_3 layer.[12]

The Mn-rich phase, observed at the $(Cr,Mn)_3O_4$/air interface in the uncoated steel has already been reported with slightly different compositions, $Cr_{1.8}Mn_{1.2}O_4$[12] and $Cr_{1.95}Mn_{1.2}O_4$.[7] The observation of a Mn-rich phase with varying compositions is attributed to two factors: (i) the outward flux due to Mn^{2+} diffusion through the spinel phase, and (ii) the chromium volatilization at the oxide scale/air interface.

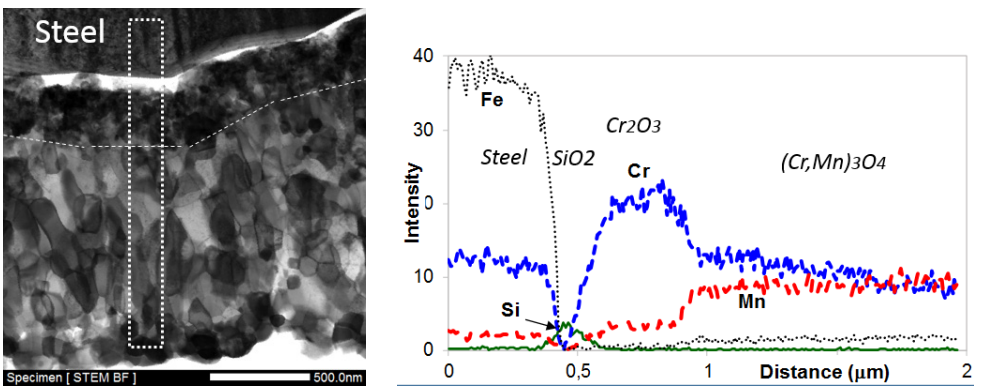

(a) (b)

Fig. 2. (a) TEM micrograph of uncoated SS446 steel after oxidation at 800°C in air for 200 h and (b) EDX profiles recorded in the rectangle.

Table 2. Grain sizes measured at TEM cross-section samples of the chromia scale and the $(Mn,Cr)_3O_4$ spinel from uncoated SS446 after 200 h oxidation in air.

	Spinel grain sizes (nm)		Chromia grain sizes (nm)	
Sample	Range	Mean	Range	Mean
Uncoated SS446	150–200	175	80–120	100

From the micrographs in Fig. 1, the grain sizes of the spinel and chromia scales were estimated and the results are summarized in Table 2. These data evidence that the chromia phase has a mean grain size in the nanosize range (100 nm), whereas the spinel phase exhibit a larger grain size (175 nm).

LSM-coated SS446 after oxidation for 480 h. Figure 4 depicts the effect of oxidation of the LSM-coated steel at 800°C in air for 480 h. Successive layers of silica, chromia, and spinel are observed similarly to the uncoated steel. In this sample, the amorphous SiO_2 layer is continuous and thicker than the one found in uncoated steel. The Cr_2O_3 layer (brown in Fig. 4(h)) is well identified from ACOM method except few small areas which were poorly indexed and appear in white. These latter do not fit with composition variations in the chromia layer (Figs. 4(c)–4(e)). The chromia layer is therefore considered homogeneous in this sample. A few Cr_2O_3 grains are observed in the spinel phase as for the uncoated steel. A detailed analysis of the composition in the spinel layer like in Fig. 4(g) indicates that Mn amount

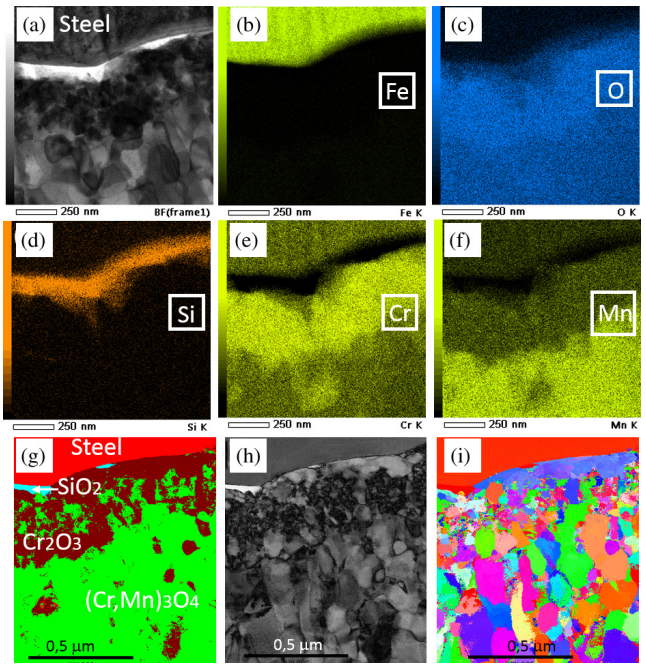

Fig. 3. Chemical and crystallographic characterization of the upper part of the oxide scale formed on the uncoated steel after 200 h at 800°C in air. (a)–(f) TEM/EDX maps. (g)–(i) Phase, phase reliability, and grain orientation maps obtained with the ACOM technique.

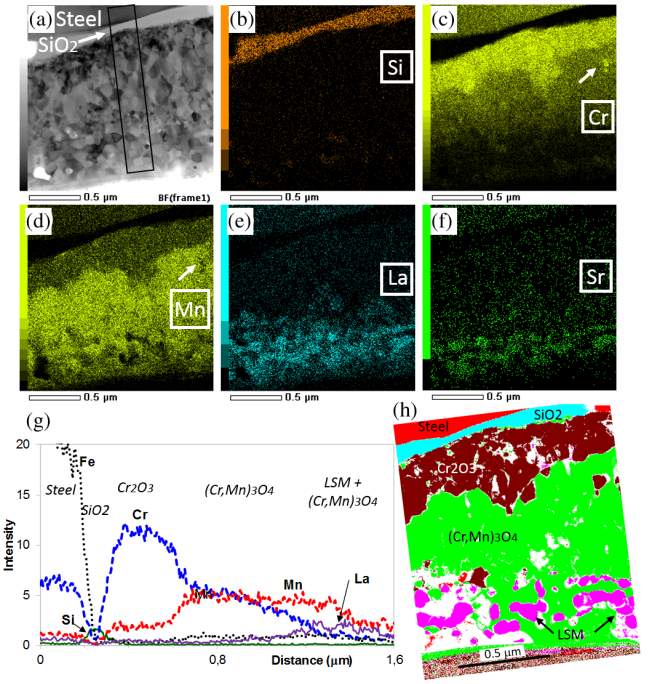

Fig. 4. (a)–(f) TEM micrograph and EDX maps of the oxide scale formed on the LSM coated steel after oxidation at 800°C in air for 480 h. (g) EDX profiles recorded in the rectangle. (h) Phase map obtained with the ACOM technique, where white areas are grains with a low phase reliability.

slightly increases towards the surface while Cr amount decreases. It results in a higher Mn content towards the surface. The outer layer consists of a mixture of LSM and spinel grains, with spinel grains in contact to the surface with air (Figs. 4(e), 4(f) and 4(h)).

Proposed transport process. Based on the above results obtained with the uncoated and LSM coated steels, the transport mechanism occurring during the annealing of the SS446 steel at 800°C in air is proposed as follows. Oxygen from the surface diffuses towards the steel contrary to Cr and Mn. These chemical diffusions result in the formation of chromium oxide scale and spinel phase. A continuous SiO_2 layer forms at the interface with steel owing to the high Si content available in the SS446 steel. SiO_2 appears amorphous that is usually considered to be a favorable state for limiting the diffusion.[13] Figure 5 shows the composition profile across the SiO_2 film for the uncoated and coated samples. We observe a pure SiO_2 film, free of Mn and Cr, in agreement with the property of the barrier layer. In the detection threshold of micrographs, traces of amorphous nanometric layer of $MnSi_xO_y$ at the interface of SiO_2 with the steel alloy were not detected contrary to the literature.[14] This layer involving SiO_2 phase and Mn alloy has been proved to act as a good diffusion interface barrier. Two different spinels progressively richer in Mn are detected in both coated and uncoated samples at the surface. The difference in the composition of these

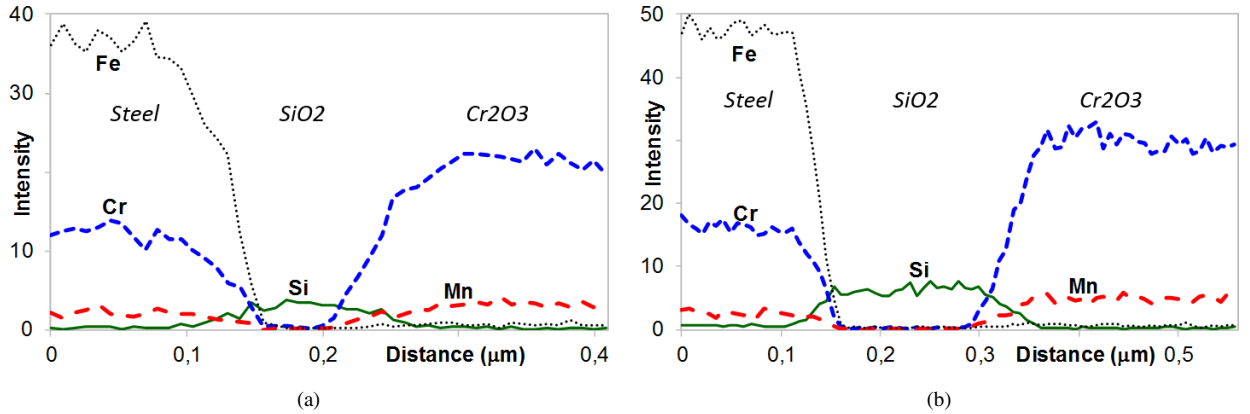

Fig. 5. Composition profile across the SiO_2 layer after oxidation in air at 800°C (a) in uncoated (200 h) and (b) in LSM coated (480 h) SS446 steel.

spinel phases comes probably from the higher diffusion rate of Mn with comparison to the Cr one.[12] A relatively low solubility of Mn in Cr_2O_3 or the Cr evaporation could be also assumed. For the LSM coated sample, a source of Mn may also arise from the LSM film.[15] The observations reveal a protective effect of the dense LSM coating after oxidation at 800°C for 480 h as it limits oxygen migration and Cr evaporation. The diffusion of manganese and lanthanum from the LSM coating likely also promotes the oxide scale growth.[16] However, after a long treatment, the LSM layer becomes discontinuous, with LSM grains surrounded by spinel grains, leading to degradation.

Microstructural characterization was performed by TEM, EDX, and electron diffraction at the surface of a SS446 steel alloy coated and uncoated by a protective LSM perovskite film as thin as 450 nm deposited by ESD. After oxidation at 800°C in air for 200 h, the uncoated SS446 steel consists of an assembly of amorphous SiO_2, Cr_2O_3, topped by $(Mn, Cr)_3O_4$ spinel grains. When the steel is coated with LSM and the oxidation extended to 480 h at 800°C, the SiO_2 layer is thicker and the growth of both chromia and spinel layers are limited. The formation of the SiO_2 amorphous layer related to the high amount of Si in the SS446 steel likely plays a significant role as a diffusion barrier. The thin LSM layer has been proved to have a beneficial effect against oxidation at 800°C in air at least up to 480 h.

Acknowledgment

The financial supports of FAPESP (2013/07296-2 and 2012/07648-3) and CNPq (476895/2012-0) are gratefully acknowledged. Electron microscopy was performed at the CMTC characterization platform of Grenoble INP, supported by the Centre of Excellence of Multifunctional Architectured Materials "CEMAM" n°ANR-10-LABX-44-01 funded by the "Investments for the Future" Program.

References

1. J. W. Fergus, R. Hui, X. Li, D. P. Wilkinson and J. Zhang, *Solid Oxide Fuel Cells: Materials Properties and Performance*, (CRC Press, Taylor & Francis Group, Boca Raton, FL, USA, 2009).
2. E. Konysheva, J. Laatsch, E. Wessel, F. Tietz, N. Christiansen, L. Singheiser and K. Hilpert, *Solid State Ion.* **177**, 923 (2006).
3. N. Shaigan, D. G. Ivey and W. Chen, *J. Power Sources* **185**, 331 (2008).
4. Y. D. Zhen, S. P. Jiang, S. Zhang and V. Tan, *J. Eur. Ceram. Soc.* **26**, 3253 (2006).
5. J. W. Fergus, *Scr. Mater.* **65**, 73 (2011).
6. L. da Conceição, L. Dessemond, E. Djurado and M. M. V. M. Souza, *J. Power Sources* **241**, 159 (2013).
7. L. da Conceição and M. M. V. M. Souza, *Thin Solid Films* **534**, 218 (2013).
8. L. da Conceição, L. Dessemond, E. Djurado and E. N. S. Muccillo, *Surf. Coat. Technol.* **254**, 157 (2014).
9. A. Princivalle and E. Djurado, *Solid State Ion* **179**, 1921 (2008).
10. E. F. Rauch and M. Véron, *Mater. Charact.* **98**, 1 (2014).
11. I.-H. Jung, *Solid State Ion.* **177**, 765 (2006).
12. S. Canovic, J. Froitzheim, R. Sachitanand, M. Nikumaa, M. Halvarsson, L.-G. Joahansson and J.-E. Svensson, *Surf. Coat. Technol.* **215**, 62 (2013).
13. C. E. Ramberga, E. Blanquet, M. Pons, C. Bernard and R. Madar, *Microelectron. Eng.* **50**, 357 (2000).
14. J. Koike and M. Wada, *Appl. Phys. Lett.* **87**, 041911 (2005).
15. M. Palcut, L. Mikkelsen, K. Neufeld, M. Chen, R. Knibbe and P. V. Hendriksen, *Int. J. Hydrog. Energy* **37**, 14501 (2012).
16. M. Palcut, L. Mikkelsen, K. Neufeld, M. Chen, R. Knibbe and P. V. Hendriksen, *Int. J. Hydrog. Energy* **37**, 8087 (2012).